HHS Public Access

Author manuscript

Am J Hematol. Author manuscript; available in PMC 2023 January 01.

Published in final edited form as:

Am J Hematol. 2022 January 01; 97(1): 18–29. doi:10.1002/ajh.26382.

Congenital X-linked Neutropenia with Myelodysplasia and Somatic Tetraploidy due to a Germline Mutation in SEPT6

Raffaele Renella[1,2], **Katelyn Gagne**[2], **Ellen Beauchamp**[3], **Jonathan Fogel**[2], **Aleksej Perlov**[2], **Mireia Sola**[10], **Thorsten Schlaeger**[2], **Inga Hofmann**[2,4,11], **Akiko Shimamura**[2], **Benjamin L Ebert**[3,9], **Klaus Schmitz-Abe**[6], **Kyriacos Markianos**[5], **Kristi Murphy**[5], **Liang Sun**[5], **Shira Rockowitz**[5], **Piotr Sliz**[5,7], **Dean R Campagna**[4], **Timothy A Springer**[8,10], **Christopher Bahl**[2,10], **Suneet Agarwal**[2,9], **Mark D Fleming**[4], **David A Williams**[2,9]

[1]Pediatric Hematology-Oncology Research Laboratory, Lausanne University Hospital, Switzerland

[2]Division of Hematology-Oncology, Boston Children's Hospital, Harvard Medical School, Boston, USA

[3]Department of Medical Oncology, Dana-Farber Cancer Institute, Harvard Medical School, Boston, USA

[4]Department of Pathology, Boston Children's Hospital, Harvard Medical School, Boston, USA

[5]The Manton Center for Orphan Disease Research, Boston Children's Hospital, Boston, USA

[6]Division of Newborn Medicine, Department of Pediatrics, Boston Children's Hospital, Boston, USA

[7]Division of Molecular Medicine, Boston Children's Hospital, Boston, USA

[8]Program in Cellular & Molecular Medicine, Boston Children's Hospital, Boston, USA

[9]Harvard Stem Cell Institute, Harvard Medical School, Boston, USA

[10]Institute for Protein Innovation, Boston, USA

[11]Present address: Division of Pediatric Hematology-Oncology, University of Wisconsin School of Medicine, Madison, USA

Abstract

Septins play key roles in mammalian cell division and cytokinesis but have not previously been implicated in a germline human disorder. A male infant with severe neutropenia and progressive dysmyelopoiesis with tetraploid myeloid precursors was identified. No known genetic etiologies

*Corresponding author: Dr David A. Williams, Division of Hematology-Oncology, Boston Children's Hospital, 300 Longwood Ave, Karp 08125.3, Boston, MA 02115, Phone: 617-919-2697, Fax: 617-730-0868, DAWilliams@childrens.harvard.edu.

Authorship contributions

RR and DAW provided medical care. RR, BLE, SA, MDF and DAW designed research. RR, KG, EB, JF, AP, TS, DC conducted experiments and acquired data. RR, IH, KSA, AS, KM, TAS, MDF, LS, KM, SR, PS, MS, CB analyzed data. RR and DAW wrote and edited the manuscript.

The authors have declared that no conflict of interest exists.

Data and Code Availability

The genomic raw data supporting the current study have not been deposited in a public repository due to the fact the related to a single individual and provide whole genome/exome information but are available from the corresponding author on request.

for neutropenia or bone marrow failure were found. However, next-generation sequencing of germline samples from the patient revealed a novel, *de novo* germline stop-loss mutation in the X-linked gene *SEPT6* that resulted in reduced SEPT6 staining in BM granulocyte precursors and megakaryocytes. Patient skin fibroblast-derived induced pluripotent stem cells (iPSCs) produced reduced myeloid colonies, particularly of the granulocyte lineage. CRISPR/Cas9 knock-in of the patient's mutation or complete knock-out of *SEPT6* was not tolerated in non-patient derived iPSCs or human myeloid cell lines, but *SEPT6* knock-out was successful in an erythroid cell line and resulting clones revealed a propensity to multinucleation. *In silico* analysis predicts the mutated protein hinders the dimerization of SEPT6 coiled coils in both parallel and antiparallel arrangements, which could in turn impair filament formation. These data demonstrate a critical role for *SEPT6* in chromosomal segregation in myeloid progenitors that can account for the unusual predisposition to aneuploidy and dysmyelopoiesis.

Introduction

The Septin proteins are members of the translation factor (TRAFAC) class of P-loop nucleotide-binding family and are functionally related to Ras-like GTPases and kinesin and myosin cytoskeletal motors[1,2]. Septins play key roles in mammalian cell division and cytokinesis and are phylogenetically conserved from yeast to humans. They are involved in cancer, ageing, infectious diseases and reproductive and neurodegenerative disorders [2-4]. The roles of individual Septins in cell division, plasma membrane receptor clustering, apoptosis, and pro-metastatic cytoskeletal component interactions have been investigated in cancer [5]. Somatic Septin mutations have been implicated in the pathogenesis of infant and early childhood acute myeloid leukemia (AML), specifically as fusion partners of the *mixed lineage leukemia* (*MLL*) gene [6-11]. *MLL-SEPT6* (11q23:Xq24) fusions produce chimeric proteins associating specifically with the product of *MLL* exons 9, 10, 11, or 12 and *SEPT6*. The *MLL*-Septin associated leukemias are phenotypically distinct from *MLL*-rearranged AML, as they tend to be confined to children below the age of 3 years, and display features without monocytic or myelomonocyte phenotype typical of *MLL*-rearranged AML.

Several murine Septin knock-out models suggest a tissue-specific role for these proteins in cytokinesis. For example, deletion of *Sept7* causes cytokinesis defects in fibroblasts, but no alterations in the proliferation and maturation of B- and T-lymphocytes, or myeloid progenitors [12]. In addition, a murine knock-out of *Sept6* has been reported to be viable and without a leukemic predisposition, providing evidence for potential redundancy within the Septin protein family [13].

Germline mutations affecting hematopoiesis cause phenotypically overlapping bone marrow failure (BMF) syndromes that can be associated with the evolution to aplastic anemia, myelodysplasia (MDS), and AML [14,15]. Recently, leukemic transformation in MDS has been shown to be associated with the accumulation of clonal subpopulations of abnormal hematopoietic stem cells (HSCs) or hematopoietic progenitor cells (HPCs). These clonal fluctuations have also been observed in certain single lineage inherited cytopenias [16-19]. Pediatric MDS differs from adult MDS both phenotypically and at the genomic level. Presentation at an early age has been associated with distinct germline and somatic

mutations involving a growing number of genes, including the *RAS*/*MAPK* pathway and *SAMD9/SAMD9L* [15,20]. Pediatric MDS associated with *SAMD9/SAMD9L*, has the unique property that it can spontaneously remit by the acquisition of a loss-of-function mutation in *cis* of the disease associated gain-of-function variant or by duplication of the wild type allele with loss of the mutant allele [21,22]. This phenomenon has very recently been termed as "somatic genetic rescue" [23]. Loss of the mutant chromosome alone, however, can result in disease progression to MDS with monosomy 7. This observation indicates that private mutations unique to individuals may themselves be clinically silent or have limited phenotypes, but can predispose to additional events, such as chromosomal loss, that cause neoplastic transformation [24].

In this study, we identified a *de novo* germline mutation in *SEPT6* in a newborn with severe neutropenia who acquired additional molecular alterations necessitating early HSCT to treat progressive MDS. We investigated the functional consequences of this mutation in myelopoiesis.

Materials & Methods

Patient material

This study was conducted according to Declaration of Helsinki principles and written informed consent was obtained from the patient's parents prior to inclusion in the study and after appropriate institutional review board at Boston Children's Hospital (Protocol 10-02-0057).

DNA sequencing and genetic analysis

We performed whole exome sequencing (WES) of the affected individual's extracted patient germline DNA from a buccal sample (BS), skin fibroblasts (SF) and bone marrow. WES for the SF and BM were performed by MACROGEN (Axeq-Macrogen, Rockville, MD) at 60x depth with baits covering ~60 Mb of the genome. We performed whole genome sequencing (WGS) of the parent-child trio on germline DNA from SF at 40x depth (Illumina, San Diego, CA). WES for the BS was performed as previously described [25]. Sanger confirmations were performed on DNA from the peripheral blood. We leveraged multiple pipelines to automate the discovery process, the Variant Explorer (VExP) pipeline and BCH Genomics Learning System (GLS) using the human reference assembly hg19 as has been previously described [25,26]. We used a phenotype-focused strategy to look for variants that had low allele frequencies in reference databases and high or moderate variant effect prediction (VEP) in candidate genes known to play a role in hematopoietic disorders (disease-focused analysis) as well as across all genes that had variants that matched the allele frequency and VEP criteria (unbiased analysis)[27].

We performed amplicon sequencing of the SEPT6 (three5 independent pools of 15 exons for a total of ~300Mbp) in the four passages of patient cells and patient's bone marrow at the Dana-Farber Cancer Institute sequencing core. We used trimmomatic v0.39 (Bolger, Lohse, & Usadel, 2014) to trim the raw reads. The adapters and other illumina-specific sequences were cut off by using illumina provided TruSeq3-PE.fa and low-quality amplicon

sequencing data were trimmed by cutting the three bases off the start and end of a read if the average quality score of 4 bp sliding window fails below the threshold 15. The minimal size of trimmed read should be 36 bp. High-quality reads were aligned to the human reference genome (GRCh38.v32) using STAR 2.7.2b (Dobin et al., 2013). VarScan2 (Koboldt et al., 2012) were used to detect SNPs and INDELs of the targeted gene SEPT6. We used liftOver (https://genome.ucsc.edu/cgi-bin/hgLiftOver) from UCSC to convert the variants identified from GRCh38 to hg19 for comparison with the WES and WGS data.

Transcriptome sequencing and analysis

We extracted RNA from whole BM and performed RNA sequencing of the patient and one normal control by MACROGEN (Axeq-Macrogen, Rockville, MD). To keep only high-quality reads for analysis, we use trimmomatic v0.39 (Bolger, Lohse, & Usadel, 2014) to trim the NGS reads using the same parameters as the amplicon sequencing analysis. The high-quality trimmed reads were aligned to the human reference genome (GRCh38.v32) using STAR 2.7.2b (Dobin et al., 2013). At RNA sequencing, we were able to confirm that the M2 variant did not cause alternative splicing or non-canonical isoforms. GFOLD software (Feng et al., 2012) was used to identify differentially expressed genes (gfold value >= 5 or gfold value <= − 5). KEGG pathways and gene ontology (GO) enrichment tests were performed by the clusterProfiler R package (Yu, Wang, Han, & He, 2012). A pathway or GO term was treated as significantly enriched if an adjusted p-values (with Benjamini-Hochberg correction) was smaller than 0.05.

Cell lines

TF-1 cells were cultured in RPMI 1640 (Corning; New York, NY) supplemented with 10% heat-inactivated fetal bovine serum (Omega Scientific, Tarzana, CA) and 1% penicillin, streptomycin, and l-glutamine (Gibco, Waltham, MA), plus 2 ng/ml recombinant human GM-CSF (Miltenyi Biotec, Bergisch Gladbach, Germany).

iPSC generation, culture and characterization

Derivation, culture, characterization, and differentiation of iPSCs were as performed as described by Park et al. [28]. iPSC lines were cultured on human embryonic stem cell (hESC)-qualified Matrigel (BD Biosciences, Franklin Lakes, NJ), and passaged every 6–7 days, with manual removal of differentiated cells under a dissecting microscope, release of colonies with Collagenase IV (Invitrogen, Grand Island, NY), and fragmentation and collection using a cell scraper. Pluripotency was assessed by immunofluorescence as described by Chan et al. [29]. Teratomas were generated as described by Park et al. [30] and intramuscular injection of iPS cells in immunodeficient mice included in protocols approved by the institutional review board at Boston Children's Hospital. Histology was performed at the Dana-Farber Harvard Cancer Center Rodent Histopathology core facility.

Hematopoietic colony forming assays

iPSCs were collected as large aggregates and resuspended in embryoid body (EB) differentiation medium (80% DMEM, 20% fetal calf serum, 50 ug/ml ascorbic acid, and 0.2 ug/ml holo-transferrin) on low attachment dishes. After 1 day, cytokines were added:

hSCF (300 ng/ml), hFlt3L (300 ng/ml), IL-3 (10 ng/ml), IL-6 (10 ng/ml), G-CSF (50 ng/ml), and BMP4 (50 ng/ml). Media containing cytokines were replaced every 3 days for 14–16 days, as described by Cerdan et al. [31]. EBs were dissociated and equal number of cells was plated in MethoCult GF H4434 complete methylcellulose medium (Stem Cell Technologies, Vancouver, Canada). After 14–16 days of hematopoietic differentiation, CFU colonies were counted by two experienced observers who were blind to the identity of the samples. For CFU qualification, colonies picked from methylcellulose were washed in phosphate buffered saline (PBS), plated on glass slides by cytospin, and stained using MGG.

CRISPR/Cas9 knock-in and knock-out experiments

The pL-CRISPR.EFS.GFP vector (Addgene, Watertown, MA) was used for CRISPR-Cas9 experiments, and guide RNAs (gRNAs) were cloned into the vector using a BsmBI restriction site. gRNA sequences are listed in Supplementary Table 1. HL-60, Molm13, and TF-1 cells were lentivirally transduced with the pL-CRISPR.EFS.GFP vector containing the gRNA of interest. 3 days post transduction, transduced cells with high green fluorescent protein (GFP) expression were fluorescence-activated cell sorted (FACSAria II; BD Biosciences). Cells were expanded, and genotyping was performed by PCR amplifying 200-300bp of genomic sequence spanning the predicted Cas9 cut site, followed by deep sequencing performed by the CCIB DNA Core Facility at Massachusetts General Hospital (Cambridge, MA). For the TF-1 cell line transduced with gRNA #1, single-cell clones were generated by limiting dilution and were genotyped to identify clones with frameshift insertions or deletions. Clones with a 7 bp deletion were used for experiments.

Antibodies & Reagents

qPCR primers were drawn from the MGH-PrimerBank [32], and gRNA sequences for CRISPR/Cas9 experiments are provided in Supplementary Table 5. Antibodies are described in the Supplementary Table 6.

In-silico analysis

Models of the monomeric form of the A-I and M2 mutated isoforms of Septin6 were generated using the neural network-based AlphaFold2 structure prediction method. We also modeled the parallel coiled-coil dimer of Sept6 using the CCFold web server [33]. Next, the modelled monomers of both isoforms were aligned to the crystal structure of the antiparallel Sept6 dimer (PDB 6wbp) or the modeled parallel dimer. The dimeric models were refined using Rosetta FastRelax via the RosettaScripts application programming interface (Fleishman et al. 2011) with coordinate constraints applied to the Cα atoms [34,35]. Finally, these refined dimeric models were evaluated using the Rosetta-ICO energy function [36]. The energy of dimer formation (ΔΔG) was calculated by using the Rosetta ddG filter. For each model, 100 iterations were performed, and the obtained values were plotted using the ggplot2 package from R [37].

Results

Identification of a novel de novo germline SEPT6 stop-loss mutation in a patient with severe congenital neutropenia rapidly progressing to MDS

A non-dysmorphic Caucasian newborn male with a non-contributory family history presented with severe neutropenia associated with dysmyelopoiesis and tetraploidy (Figures 1 and 2). The pregnancy ($P_2G_2A_0$) was uncomplicated, the delivery unremarkable and there was no family history of blood diseases. The finding of neutropenia was incidental, and the absolute neutrophil count (ANC) was 0.5 G/L at birth, subsequently 0-0.2 G/L (Supplementary Figure S1). Initial investigations ruled out acquired etiologies and the patient was given a short trial of granulocyte colony stimulating factor (G-CSF 5 micrograms/kg/every other day for 3 months) without response. He was referred to our institution for additional diagnostic evaluation and treatment. In our clinic, he had a normal exam and evaluation for syndromic causes of neutropenia was negative. However, erythrocyte macrocytosis with an abnormally elevated fetal hemoglobin (HbF 13% at 6.5 months and 15% at 10 months of age, normal vitamin B12 and folate levels) prompted additional work-up for bone marrow failure (BMF) including a bone marrow aspiration and biopsy. These demonstrated a cellular marrow with frequent giant, dysplastic multinucleated myeloid precursors and occasional dysplastic erythroid elements (Figure 2 panel A-F, and Supplementary Data 1). Sanger sequencing of HAX1/ELANE2/GCSFR/GFI was wild-type, telomere length measurements were normal for dyskeratosis congenita/telomeropathies, a chromosomal breakage test was normal for Fanconi anemia. The patient developed progressive, clonal aberrations, including trisomies of chromosomes 7, 8 and 9 and increasing tetraploidy (Supplementary Data 1). Due to the concern of leukemic transformation and progressive cytopenias, at age 1 year he underwent an allogeneic HLA-DQ-mismatched unrelated HSCT after busulfan-cyclophosphamide/anti-thymocyte globulin (ATG) conditioning. He is currently 10 years post-HSCT with normal trilineage hematopoiesis, full donor chimerism, no graft versus host disease, and no other non-hematological or systemic phenotypes, including no evidence of organ dysfunction or cognitive impairment.

To further investigate the possible molecular etiology of this phenotype, with informed consent, whole genome sequencing (WGS) of skin fibroblast (SF) DNA from the patient and his parents and whole exome sequencing (WES) of the proband's buccal swab cells (BS), SF and BM was performed. In all WES/WGS samples, we identified a *de novo* hemizygous germline stop-loss variant in exon 10 of *SEPT6* in the proband WES/WGS data (NM_145799.3/NM_145800.3, c.1282T>C, p.*428Glnext*9, hereafter referred to as the M2-mutation). A second heterozygous stop-gain variant in exon 2, (NM_145799.3/NM_145800.3, c.43C>T, p.Arg15*, termed the M1-mutation) was present at a variant allele frequency of 14% (5/36) in the BM WES, but in none of the SF and BS WES reads, and was inferred to be somatic in origin (Figure 3 and Supplementary Table S7). This finding was validated in amplicon-based next generation resequencing of all *SEPT6* exons. Since *SEPT6* is an X-linked gene, the somatic stop-gained variant was judged to be *in cis* of the stop-loss allele. Since no wild-type sequences could be identified in the patient's skin fibroblasts, bone marrow or peripheral blood (Supplementary Table 7), germline mosaicism

was excluded, and the M1 and M2 mutations were judged to be *in cis* in the proband. In the setting of X chromosome duplication in a tetraploid clone, the event would involve a germline mutant X chromosome. Neither the M1 nor the M2 variants were present in any of the maternal or paternal samples (Supplementary Table 7). Furthermore, neither variant has previously been observed in gnomAD and the gene is flagged in gnomAD as mutation intolerant (13.5 LOF mutations expected, 1 observed, pLI = 0.9494). Furthermore, the M1 mutation was not identified in the Catalogue of Somatic Mutations in Cancer (COSMIC, https://cancer.sanger.ac.uk/cosmic). Neither phenotype-biased, nor unbiased analyses of the trio WGS or comparison the BM and FB WES yielded any other plausible variants that would explain the patient's phenotype (Supplementary Data 2, 3 and 4). RNA sequencing (RNAseq) of patient and control BM confirmed that the M2 mutation generated a novel transcript with an open reading frame that included sequences in the 3'UTR; transcripts containing the M1 stop-gained variant were also detected by RNAseq. We did not identify any evidence of alternative transcription by aberrant splicing caused by the M2 mutation. Given that *SEPT6* is implicated in myeloid leukemia and that members of the Septin family are required for cytokinesis, the *de novo* germline stop-loss M2-mutation was considered a strong causative candidate for the neutropenia and the predisposition to myeloid aneuploidy observed in the patient. Furthermore, the somatic stop-gain M1 mutation suggested that the germline variant might be under negative selective pressure.

RNAseq of the patient's BM prior to HSCT compared with that of a control, demonstrated1806 differentially expressed genes (Supplementary Table S1), amongst them, 1771 were up-regulated, and 35 down-regulated. GO analysis for biological processes identified neutrophil activation, neutrophil degranulation, neutrophil migration, myeloid leukocyte differentiation and migration, positive regulation of cytokine production as significantly enriched (Supplementary Figure S7 and Supplementary Table S3); GO analysis for molecular functions showed increased cytokine/receptor activity (Supplementary Table S4). We performed KEGG and GO enrichment analysis to dissect the functional impact of the *SEPT6* mutation. KEGG pathway analysis highlighted cytokine-cytokine receptor interaction, IL-17 signaling, and osteoclast differentiation pathways as upregulated (Supplementary Table S2). All the above-mentioned processes can directly be linked to the phenotype observed in the patient.

The SEPT6 M2 mutation (p.*428Glnext*9) alters SEPT6 *protein expression*

To assess the impact of the SEPT6 variants on protein expression and localization, we performed immunohistochemical (IHC) staining of control and patient-derived BM biopsies (Figure 2 G-H). In the BM of healthy individuals, SEPT6 staining was found to be limited to myeloid progenitors and megakaryocytes, further suggesting a potential putative link of *SEPT6* mutations with a myeloid phenotype (Supplementary Figure S6). The patient BM (Figure 2G), however, showed markedly reduced SEPT6 staining in megakaryocytes and granulocyte precursors compared to controls. The loss of staining could be attributed to instability of the stop-loss variant and/or loss of protein expression secondary to the somatic frameshift variant; the former is favored, as the allele fraction of the presumptive somatic null allele was much lower than the proportional loss of staining. Normal SEPT6 staining pattern was restored post-HSCT in the patient (Figure 2H).

The hematopoietic potential of patient-derived iPSCs

To more definitively assess the hematopoietic potential of *SEPT6* mutated cells, we generated patient and control skin fibroblast-derived induced pluripotent stem cells (iPSCs, Supplementary Figure 2) using standard methods of lentivirus-mediated expression of pluripotency genes and single cell clone selection [28,38]. Patient-derived iPSC clones had no growth or morphological differences compared with control clones except for minimal changes in colony boundaries (Supplementary Figure 2A). Two patient (C5 & C8) and two control (C1 & C6) iPSC clones underwent fidelity testing using teratoma formation assays (Supplementary Figure 2B), high-resolution karyotyping (Supplementary Figure 2C), and 16-marker immunofluorescence (IF, Supplementary Figure 2D) staining. We confirmed the presence of the *SEPT6* mutation in the patient-derived colonies by Sanger sequencing (Supplementary Figure 3A). To exclude genetic heterogeneity resulting from the iPSC-derivation or a functional impact of the mutation itself, we also performed DNA analysis of pooled iPS-derived colonies. As the p.*482Gln*9 germline variant abrogates a HpaI restriction site, we verified the presence of the mutation by genomic PCR amplification of the locus followed by HpaI digestion and agarose gel electrophoresis (Supplementary Figure 3B). In immunodeficient nude mice the iPSCs-derived teratomas contained cells from all three embryonic layers demonstrating *in vivo* pluripotency and were morphologically similar to teratomas derived from control cell lines (Supplementary Figure 1B). The iPSC clones had a normal 46 XY karyotype and expressed *bona-fide* markers of iPSCs by immunofluorescence (Supplementary Figure 2C-D). Expression of *SEPT6* mRNA and SEPT6 protein levels in iPSCs were assayed by qPCR (Supplementary Figure 4A) and Western blotting (Supplementary Figure 4B) and showed no differences between patient-derived iPSCs and healthy controls. We next studied the hematopoietic potential of these iPSCs clones using embryoid bodies (EB) formation (Supplementary Figure 2A) and colony forming assays in cytokine-supplemented methylcellulose cultures (Figure 4) as previously described [39]. Control iPSCs generated morphologically normal erythroid and myeloid colonies and cells (Figure 4A). In contrast, the patient-derived iPSCs demonstrated a significant reduction in production of myeloid progenitors; CFU-G/M/GM colonies were also markedly smaller than controls. There was a differential effect on the myeloid/granulocyte lineage compared to the erythroid lineage, with a reduction of 36-fold in CFU-G, 46-fold in CFU-GM, but only 6-fold reduction in BFU-E colonies in the patient-derived iPSC-HPC when compared to controls (Figure 4B). Thus, *in vitro* iPSCs derived hematopoietic differentiation phenocopies the patient's hematopoiesis, both qualitatively and quantitatively.

SEPT6 deficiency in an erythroleukemic cell line leads to multinucleation

To further assess the pathogenic nature of the mutation, we attempted to generate a knock-in of the patient's stop-loss mutation in iPSCs. Despite multiple approaches, CRISPR/Cas9 knock-outs and knock-ins of the p.*482Gln*9 allele (M2 mutation) was not tolerated in iPSCs or in human myeloid cell lines (HL-60, Molm-13, K562). However, we were able to generate a *SEPT6* knockout in the human erythroleukemia cell line TF-1. We analyzed these cells by cytomorphology and DNA and cell cycle assays. Both bulk and clonal populations lacked expression of SEPT6 (Supplementary Figure 5A and 5B) and individual *SEPT6* knockout TF-1 clonal lines revealed a propensity to multi-nucleation with a striking

population of giant multi-nucleated cells at low frequency, similar to those observed in the patient's BM (Figure 4C). When assayed for proliferative potential, we found no significant differences between *SEPT6* knockout TF-1 clonal lines and wild-type controls.

In-silico analysis reveals a multifactorial impact of the patient mutation on Septin6 function

SEPT6 (isoform A-I, NM_145799.4) is composed of an N-terminal G domain (residues 1-306) and a C-terminal domain (residues 307-427); the crystal structure of the former domain has been determined previously. The C-terminal domain has been proposed to play a key role in Septin filament stabilization, bundling, bending, and/or interactions with non-Septin molecules. In addition, SUMOylation of SEPT6 in this region appears to regulate Septin filament bundling and cytokinesis [40].

The M2 variant is predicted to extend the C-terminus of the A-I/III splice variant (NM_145800.4) of SEPT6 by 9 residues (Figure 3A), most of which are hydrophobic. Interestingly, two splice variants (isoforms B and D, Figure 3A) extend the same terminus by 2 and 7 residues respectively and add hydrophobic residues. This suggests a functional role and possible cell-specificity for splice variants with short C-terminal extensions, an effect largely mediated by N- and C-termini variability in Septins [41].

To better understand the effect of the M2 variant on the SEPT6 structure, we generated homology models of the human A-I and M2 isoforms using AlphaFold [42]. In both cases, the C-terminal domain forms an extended coiled-coil that is connected to the structured N-terminal through a short flexible loop (Figure 3B). This flexible loop likely "hinges" in solution, enabling the coiled-coil and G domains to sample different angles with respect to one another. This may explain why the C-terminal domain could not be resolved in previous X-ray crystallization studies [43].

Interestingly, the wild-type human SEPT6 (isoform A-I) coiled-coil exhibits a short disordered tail on its C-terminus, while in our models the 9 residues that are added by the M2 mutation form a structured motif with a clear helix propensity (Figure 3B). Based on this observation, we reasoned that this additional motif might affect the oligomerization of the human M2 mutated SEPT6 coiled coils.

To test this hypothesis, we aligned our AlphaFold models to the X-ray crystal structure of a SEPT6 antiparallel homodimer (residues 344-399) and used the Rosetta energy function to evaluate the resulting dimers (Figure 3C)[36,44]. Strikingly, the total energy and binding energy ($\Delta\Delta G$) of the human SEPT6 A-I dimer are more favorable than those of the M2 mutated isoform, indicating a higher stability of the wild-type isoform. In addition, the $\Delta\Delta G >> 0$ of the M2 mutated isoform suggests that dimer formation would likely not occur in this conformation.

Although no crystal structures of parallel SEPT6 dimers exist, SEPT6 coiled-coils are predicted to form homo- and hetero- dimers in both parallel and antiparallel arrangements, and all conformations seem to be involved in the formation of Septin filaments [44]. To assess whether the M2 mutated also affects the formation of parallel dimers, we aligned our

AlphaFold models on a parallel SEPT6 dimer obtained using the CCFold web server, and scored the resulting dimers using Rosetta [33]. Similar to our observations in the antiparallel dimer, both total energy and ΔΔG are more favorable for the wild-type human A-I than for the mutant M2 isoform (Figure 3C).

Overall, our *in-silico* analysis suggests that the *de novo* germline stop-loss *SEPT6* mutation (M2) found in the patient hinders the dimerization of SEPT6 coiled coils in both parallel and antiparallel arrangements, which could in turn impair filament formation. Nonetheless, we aligned our AlphaFold models using static, single-register structures, whereas coiled-coils are likely more flexible and different registers might coexist in solution. In these conditions, we cannot exclude the possibility that the M2 isoform adopts alternative conformations that still allow to form energetically favorable dimers. In the future, it will be important to experimentally test the oligomerization state of the M2 isoform.

Discussion

Septins are a highly conserved protein family composed of 13 mammalian members which are grouped by sequence similarity into in four clusters wherein members may reciprocally provide functional redundancy [2-4,45]. These include SEPT2 (SEPT1-2-4-5), SEPT6 (SEPT6-8-10-11-14), SEPT7, and SEPT9 (SEPT3-9-12). Structurally, Septins contain a nucleotide-binding domain and sequence motifs that interact with the phosphate groups of GTP or ATP. In contrast to the majority of Septins, members of the SEPT6 group are reported to be GTPase-deficient and remain constitutively bound to GTP which implies changes in expression levels likely regulate SEPT6 function in cells. The nucleotide binding domains are flanked by a N-terminal proline-rich membrane-interacting region and the C-termini have a coil-coiled domain [43]. Mammalian Septins form polymers and paired filaments and bind to cellular proteins in a specific manner. Expression of Septins has been shown to be developmental stage- and tissue-specific which is suggested to be largely mediated by N- and C-termini variability [41]. The C-terminus protrudes orthogonally from the filament axis and plays a key role in filament stabilization, bundling, and bending and/or in interactions with non-Septin molecules. In addition, it was recently shown that the amphipathic helix located at the very C-terminus of Cdc12, a Septin homolog in S. cerviseae, is necessary and sufficient for monomeric Septins to sense different membrane lipid compositions and curvatures defining cell shape [46].

We investigated a newborn with a unique non-syndromic phenotype of congenital neutropenia with red cell macrocytosis and a predisposition to aneuploidy that progressed to MDS. We identified a *de novo* novel germline SEPT6 C-terminal mutation and provide evidence supporting its causative role in the disease phenotype. We confirmed the correction of protein expression in myeloid progenitors after HSCT, and further amplicon sequencing showed preserved transcription without evidence of alterative splicing. RNA sequencing revealed a significant impact on neutrophil development and function, in alignment with the patient's phenotype. By generation of iPSCs and examination of derived hematopoietic progenitors, we confirmed the germline nature of the mutation and the derived iPSCs produced a similar hematopoietic phenotype *ex vivo*. These iPSCs developed normally in standard germline assays but demonstrated significantly altered

hematopoietic cell development. The hematopoietic-restricted nature of the phenotype *in vitro* is consistent with the lack of any extra-hematopoietic anomalies in the patient, his successful treatment with HSCT and benign post-HSCT course. In addition, the abnormal levels and localization of SEPT6 in the patient's BM were corrected after HSCT, further supporting the hematopoietic nature of this patient's disorder. We further functionally validated an impact of *SEPT6* mutations in myelopoiesis by gene editing by CRISPR/Cas9 to create a knockout of the gene in TF-1 cells [47]. In these GM-CSF-dependent knockout erythroleukemia cells, we observed an increased frequency of multinucleation, strongly supporting a role for *SEPT6* in cytokinesis in hematopoietic cells. Furthermore, *in silico* analysis suggests the patient mutation hinders the dimerization of SEPT6 coiled coils in both parallel and antiparallel arrangements, which could in turn impair filament formation.

This study implicates a germline disorder of *SEPT6* in a hematopoietic-restricted phenotype largely involving the myeloid lineage. Previously, significant abnormalities have been observed in bone and blood of homozygous and hemizygous Sept6 knockout mice. More importantly, *SEPT6*-MLL fusions are associated with infant AML, though its specific role not well understood [7,8,13,48]. In very young children *MLL*-rearrangements are associated with lymphoblastic phenotypes, whereas the *MLL-SEPT6* translocation results in AML [6-11]. This observation concurs with our findings highlighting a clear skewing for myeloid dysfunction in SEPT6 disruption. Moreover, MLL-SEPT2 fusions are restricted to therapy related MDS/AML, t-AML or t-MDS, suggesting a role for Septins in MDS/AML, as in our case where dysplastic signs were immediately apparent.

Furthermore, in *MLL-SEPT6*-associated AML, the *MLL-SEPT6* fusion generates chimeric fusion proteins, where the approximately entire open reading frame of *SEPT6* is merged with the *MLL* N-terminal domain. It has been debated how these fusions contribute to AML occurrence, and the data suggests that these transcripts are not directly leukemogenic. While our observations hint at a role for the fusions of *MLL-SEPT6* in disruption of myeloid cytokinesis creating a fertile ground for proper leukemogenesis mediated by second/driving genetic hits, the *MLL-Septin* leukemias have as a group not been associated with other aneuploidies, and further studies are clearly needed on the role of Septins in myelopoiesis and MDS/AML.

Our results also support the view that private and *de novo* germinal mutations in genes associated with essential cellular functions in hematopoiesis can be a predisposing factor for the development of early childhood hematological malignancy [49]. The patient acquired not only progressive cytogenetic aberrations but also appeared to develop additional somatic mutations in the same *SEPT6* gene abrogating protein expression. Interestingly, the low frequency somatic *SEPT6* stop-gain mutation (Figure 3, mutation M1) found in the patient's somatic BM pre-HSCT would abolish the deleterious effects of the germline stop-loss M2 mutation by abrogating expression of the full SEPT6 protein. Such somatic compensatory phenomenon has been observed in congenital MDS with *SAMD9/SAMD9L* germline mutations where the clonal loss of chromosome 7 achieves the same effect[23].

A limitation of our study is the refractoriness of iPSCs, HSCs and myeloid cells (primary and cell lines) to the modification of *SEPT6*, although it has not been identified in recent

screening experiments for essential genes [50]. Loss or C-terminal mutation of SEPT6 was not tolerated in multiple hematopoietic cell lines and in iPSCs, which might suggest either very specific regulatory elements and resulting expression patterns or redundancy of Septin group members is critical for SEPT6 function in specific cells. These data are also consistent with the lack of mutations resulting in haploinsufficiency of *SEPT6* in the publicly available datasets [51]. It is also worth noting that TF-1 cells are *TP53* deficient which may provide a permissive environment for the *SEPT6* mutation which otherwise was found to be intrinsically deleterious[52].

The role of G-CSF treatment cannot formally be dissected from the patient's evolution as its use has been associated with myeloid tetraploidy [53]. In this case, a bone marrow aspirate/biopsy was not performed prior treatment with G-CSF, and the patient was referred to us 3 months after this therapy had been stopped due to failure of an ANC response. We nonetheless believe that the exposure's short duration, its low therapeutic dosing and the lack of the patient's response argue against any significant contribution to the observed unfavorable clonal evolution. One single case with tetraploid hematopoiesis has previously been described in the literature believed to be caused by germline mutation of *GFI1* [54]. We did not identify any mutations in *GFI1* in BM or in the germline of the patient reported here. Moreover, the hematological phenotype detailed in the previous report was significantly different, including the age at presentation and stability of cytogenetically aberrant BM clones over time. We have no evidence to support any biological connection between these phenotypes.

A recent study longitudinally examining samples of patients with MDS who progressed to AML by targeted and single-cell NGS described the evolution of pre-MDS HSCs [19]. Within these rare populations, distinct subclones were shown to contribute to the generation of MDS blasts and/or progression to AML, providing significant contextual relevance to the study reported here. Interestingly, three patients out of seven included had somatic mutations in *SEPT* family genes. Among these, two had *SEPT6* variants, with one displaying concomitant *SEPT6* and *SEPT9* mutations predicted to have functional impact. Both *SEPT6* mutated clones were identified in the pre-MDS phase, but not subsequently. Taken in perspective, our results underline the importance of understanding the genetic events preceding pediatric MDS. Identifying novel class drugs interfering with the disruption of SEPT6 cluster function in myeloid tissue is likely to provide clues for further *in vivo* targeting of subtypes of vulnerable MDS and/or AML. Our work is particularly relevant as unrelated evidence is arising on the role of therapeutic interventions preventing the development AML [55].

In summary, we suggest that the mutation of the C-terminus of human SEPT6 causes aberrant cytokinesis and leads to a severe congenital neutropenia with tetraploidy and erythrocyte macrocytosis. We provide evidence that Septin proteins play key roles in mammalian cell division and cytokinesis and highlight a role for *SEPT6* in myelopoiesis. The resulting genomic instability is associated with progressive MDS and cytogenetic aberrations. This constitutes a paradigm for private germline mutations of genes affecting basic cellular functions in hematopoiesis, but not driving leukemic transformation directly.

Further investigations are warranted to elucidate the role of Septins in normal and disordered hematopoiesis.

Supplementary Material

Refer to Web version on PubMed Central for supplementary material.

Acknowledgments

We thank Chad Harris and Katia Balmas-Bourloud for technical assistance, and the Bone Marrow Failure Clinic Team at Boston Children's Hospital for their logistical support. We thank Dr David G Nathan, VG Sankaran and Olaf Bodamer for critical advice. We thank Mursal Hassan for help in manuscript preparation. This work was supported by the Amy Clare Potter Fellowship (RR) and the NIH-NIDDK-5R24DK099808 grant (AS, KM, MDF, DAW).

References

1. Kinoshita M, Field CM, Coughlin ML, Straight AF, Mitchison TJ. Self- and actin-templated assembly of Mammalian septins. Developmental cell. 2002;3(6):791–802. [PubMed: 12479805]
2. Caudron F, Yadav S. Meeting report - shining light on septins. J Cell Sci. 2018;131(1).
3. Nishihama R, Onishi M, Pringle JR. New insights into the phylogenetic distribution and evolutionary origins of the septins. Biol Chem. 2011;392(8-9):681–687. [PubMed: 21824002]
4. Dolat L, Hu Q, Spiliotis ET. Septin functions in organ system physiology and pathology. Biol Chem. 2014;395(2):123–141. [PubMed: 24114910]
5. Pous C, Klipfel L, Baillet A. Cancer-Related Functions and Subcellular Localizations of Septins. Front Cell Dev Biol. 2016;4:126. [PubMed: 27878118]
6. Cerveira N, Bizarro S, Teixeira MR. MLL-SEPTIN gene fusions in hematological malignancies. Biological chemistry. 2011;392(8-9):713–724. [PubMed: 21714766]
7. Cerveira N, Micci F, Santos J, et al. Molecular characterization of the MLL-SEPT6 fusion gene in acute myeloid leukemia: identification of novel fusion transcripts and cloning of genomic breakpoint junctions. Haematologica. 2008;93(7):1076–1080. [PubMed: 18492691]
8. Ono R, Taki T, Taketani T, et al. SEPTIN6, a human homologue to mouse Septin6, is fused to MLL in infant acute myeloid leukemia with complex chromosomal abnormalities involving 11q23 and Xq24. Cancer research. 2002;62(2):333–337. [PubMed: 11809673]
9. Slater DJ, Hilgenfeld E, Rappaport EF, et al. MLL-SEPTIN6 fusion recurs in novel translocation of chromosomes 3, X, and 11 in infant acute myelomonocytic leukaemia and in t(X;11) in infant acute myeloid leukaemia, and MLL genomic breakpoint in complex MLL-SEPTIN6 rearrangement is a DNA topoisomerase II cleavage site. Oncogene. 2002;21(30):4706–4714. [PubMed: 12096348]
10. Kim HJ, Ki CS, Park Q, et al. MLL/SEPTIN6 chimeric transcript from inv ins(X;11)(q24;q23q13) in acute monocytic leukemia: report of a case and review of the literature. Genes Chromosomes Cancer. 2003;38(1):8–12. [PubMed: 12874781]
11. Santos J, Cerveira N, Bizarro S, et al. Expression pattern of the septin gene family in acute myeloid leukemias with and without MLL-SEPT fusion genes. Leukemia research. 2010;34(5):615–621. [PubMed: 19748670]
12. Menon MB, Sawada A, Chaturvedi A, et al. Genetic Deletion of SEPT7 Reveals a Cell Type-Specific Role of Septins in Microtubule Destabilization for the Completion of Cytokinesis. PLoS Genetics. 2014;10(8):e1004558. [PubMed: 25122120]
13. Ono R, Ihara M, Nakajima H, et al. Disruption of Sept6, a fusion partner gene of MLL, does not affect ontogeny, leukemogenesis induced by MLL-SEPT6, or phenotype induced by the loss of Sept4. Molecular and Cellular Biology. 2005;25(24):10965–10978. [PubMed: 16314519]
14. Churpek JE. Familial myelodysplastic syndrome/acute myeloid leukemia. Best Pract Res Clin Haematol. 2017;30(4):287–289. [PubMed: 29156196]

15. Babushok DV, Bessler M, Olson TS. Genetic predisposition to myelodysplastic syndrome and acute myeloid leukemia in children and young adults. Leuk Lymphoma. 2016;57(3):520–536. [PubMed: 26693794]
16. Bowman RL, Busque L, Levine RL. Clonal Hematopoiesis and Evolution to Hematopoietic Malignancies. Cell Stem Cell. 2018;22(2):157–170. [PubMed: 29395053]
17. Link DC, Kunter G, Kasai Y, et al. Distinct patterns of mutations occurring in de novo AML versus AML arising in the setting of severe congenital neutropenia. Blood. 2007;110(5):1648–1655. [PubMed: 17494858]
18. Makishima H, Yoshizato T, Yoshida K, et al. Dynamics of clonal evolution in myelodysplastic syndromes. Nat Genet. 2017;49(2):204–212. [PubMed: 27992414]
19. Chen J, Kao YR, Sun D, et al. Myelodysplastic syndrome progression to acute myeloid leukemia at the stem cell level. Nat Med. 2018.
20. Schwartz JR, Ma J, Lamprecht T, et al. The genomic landscape of pediatric myelodysplastic syndromes. Nat Commun. 2017;8(1):1557. [PubMed: 29146900]
21. Davidsson J, Puschmann A, Tedgard U, Bryder D, Nilsson L, Cammenga J. SAMD9 and SAMD9L in inherited predisposition to ataxia, pancytopenia, and myeloid malignancies. Leukemia. 2018;32(5):1106–1115. [PubMed: 29535429]
22. Pastor VB, Sahoo SS, Boklan J, et al. Constitutional SAMD9L mutations cause familial myelodysplastic syndrome and transient monosomy 7. Haematologica. 2018;103(3):427–437. [PubMed: 29217778]
23. Sahoo SS, Pastor VB, Goodings C, et al. Clinical evolution, genetic landscape and trajectories of clonal hematopoiesis in SAMD9/SAMD9L syndromes. Nature Medicine. 2021.
24. Turner TN, Coe BP, Dickel DE, et al. Genomic Patterns of De Novo Mutation in Simplex Autism. Cell. 2017;171(3):710–722 e712. [PubMed: 28965761]
25. Rockowitz S, LeCompte N, Carmack M, et al. Children's rare disease cohorts: an integrative research and clinical genomics initiative. NPJ Genom Med. 2020;5:29. [PubMed: 32655885]
26. Schmitz-Abe K, Li Q, Rosen SM, et al. Unique bioinformatic approach and comprehensive reanalysis improve diagnostic yield of clinical exomes. Eur J Hum Genet. 2019;27(9):1398–1405. [PubMed: 30979967]
27. McLaren W, Gil L, Hunt SE, et al. The Ensembl Variant Effect Predictor. Genome Biol. 2016;17(1):122. [PubMed: 27268795]
28. Park I-H, Lerou PH, Zhao R, Huo H, Daley GQ. Generation of human-induced pluripotent stem cells. Nature Protocols. 2008;3(7):1180–1186. [PubMed: 18600223]
29. Chan EM, Ratanasirintrawoot S, Park IH, et al. Live cell imaging distinguishes bona fide human iPS cells from partially reprogrammed cells. Nat Biotechnol. 2009;27(11):1033–1037. [PubMed: 19826408]
30. Park IH, Zhao R, West JA, et al. Reprogramming of human somatic cells to pluripotency with defined factors. Nature. 2008;451(7175):141–146. [PubMed: 18157115]
31. Cerdan C, Hong SH, Bhatia M. Formation and hematopoietic differentiation of human embryoid bodies by suspension and hanging drop cultures. Current protocols in stem cell biology. 2007;Chapter 1:Unit 1D 2.
32. Spandidos A, Wang X, Wang H, Seed B. PrimerBank: a resource of human and mouse PCR primer pairs for gene expression detection and quantification. Nucleic Acids Res. 2010;38(Database issue):D792–799. [PubMed: 19906719]
33. Guzenko D, Strelkov SV. CCFold: rapid and accurate prediction of coiled-coil structures and application to modelling intermediate filaments. Bioinformatics. 2018;34(2):215–222. [PubMed: 28968723]
34. Tyka MD, Jung K, Baker D. Efficient sampling of protein conformational space using fast loop building and batch minimization on highly parallel computers. J Comput Chem. 2012;33(31):2483–2491. [PubMed: 22847521]
35. Fleishman SJ, Leaver-Fay A, Corn JE, et al. RosettaScripts: a scripting language interface to the Rosetta macromolecular modeling suite. PLoS One. 2011;6(6):e20161. [PubMed: 21731610]

36. Pavlovicz RE, Park H, DiMaio F. Efficient consideration of coordinated water molecules improves computational protein-protein and protein-ligand docking discrimination. PLoS Comput Biol. 2020;16(9):e1008103. [PubMed: 32956350]
37. Wickham H. ggplot2: Elegant Graphics for Data Analysis.: Springer-Verlag New York; 2016.
38. Agarwal S, Loh Y-H, McLoughlin EM, et al. Telomere elongation in induced pluripotent stem cells from dyskeratosis congenita patients. Nature. 2010;464(7286):292–296. [PubMed: 20164838]
39. Wang L, Menendez P, Shojaei F, et al. Generation of hematopoietic repopulating cells from human embryonic stem cells independent of ectopic HOXB4 expression. The Journal of experimental medicine. 2005;201(10):1603–1614. [PubMed: 15883170]
40. Ribet D, Boscaini S, Cauvin C, et al. SUMOylation of human septins is critical for septin filament bundling and cytokinesis. J Cell Biol. 2017;216(12):4041–4052. [PubMed: 29051266]
41. Hall PA, Jung K, Hillan KJ, Russell SEH. Expression profiling the human septin gene family. The Journal of pathology. 2005;206(3):269–278. [PubMed: 15915442]
42. Jumper J, Evans R, Pritzel A, et al. Highly accurate protein structure prediction with AlphaFold. Nature. 2021.
43. Sirajuddin M, Farkasovsky M, Hauer F, et al. Structural insight into filament formation by mammalian septins. Nature. 2007;449(7160):311–315. [PubMed: 17637674]
44. Leonardo DA, Cavini IA, Sala FA, et al. Orientational Ambiguity in Septin Coiled Coils and its Structural Basis. J Mol Biol. 2021;433(9):166889. [PubMed: 33639214]
45. Garcia G 3rd, Finnigan GC, Heasley LR, et al. Assembly, molecular organization, and membrane-binding properties of development-specific septins. J Cell Biol. 2016;212(5):515–529. [PubMed: 26929450]
46. Cannon KS, Woods BL, Crutchley JM, Gladfelter AS. An amphipathic helix enables septins to sense micrometer-scale membrane curvature. J Cell Biol. 2019.
47. Kitamura T, Tange T, Terasawa T, et al. Establishment and characterization of a unique human cell line that proliferates dependently on GM-CSF, IL-3, or erythropoietin. J Cell Physiol. 1989;140(2):323–334. [PubMed: 2663885]
48. Kadkol SS, Bruno A, Oh S, Schmidt ML, Lindgren V. MLL-SEPT6 fusion transcript with a novel sequence in an infant with acute myeloid leukemia. Cancer Genetics and Cytogenetics. 2006;168(2):162–167. [PubMed: 16843108]
49. Furutani E, Shimamura A. Germline Genetic Predisposition to Hematologic Malignancy. J Clin Oncol. 2017;35(9):1018–1028. [PubMed: 28297620]
50. Wang T, Birsoy K, Hughes NW, et al. Identification and characterization of essential genes in the human genome. Science (New York, NY). 2015;350(6264):1096–1101.
51. Lek M, Karczewski KJ, Minikel EV, et al. Analysis of protein-coding genetic variation in 60,706 humans. Nature. 2016;536(7616):285–291. [PubMed: 27535533]
52. Sugimoto K, Toyoshima H, Sakai R, et al. Frequent mutations in the p53 gene in human myeloid leukemia cell lines. Blood. 1992;79(9):2378–2383. [PubMed: 1571549]
53. Kaplinsky C, Trakhtenbrot L, Hardan I, et al. Tetraploid myeloid cells in donors of peripheral blood stem cells treated with rhG-CSF. Bone Marrow Transplantation. 2003;32(1):31–34. [PubMed: 12815475]
54. Hochberg JC, Miron PM, Hay BN, et al. Mosaic tetraploidy and transient GFI1 mutation in a patient with severe chronic neutropenia. Pediatr Blood Cancer. 2008;50(3):630–632. [PubMed: 17096407]
55. Uckelmann HJ, Kim SM, Wong EM, et al. Therapeutic targeting of preleukemia cells in a mouse model of NPM1 mutant acute myeloid leukemia. Science. 2020;367(6477):586–590. [PubMed: 32001657]

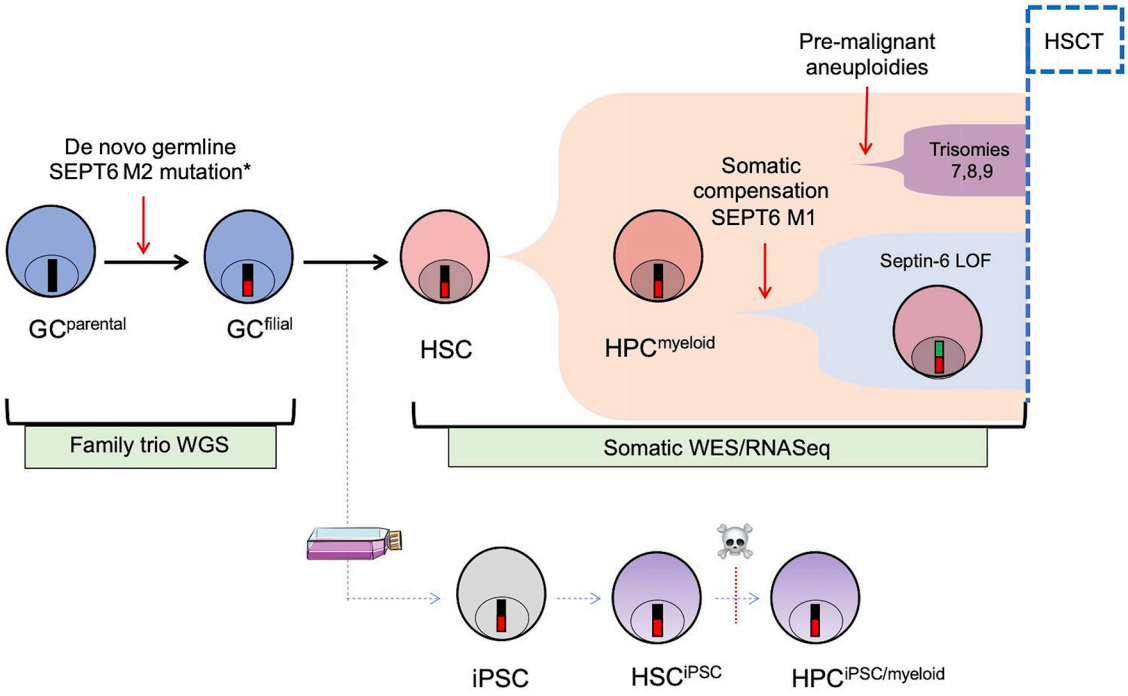

Figure 1: Schematic representation of the study.

A newborn with severe congenital neutropenia developed progressive MDS with tetraploid myeloid progenitors, and had to undergo an allogeneic HSCT before age 1 y.o. He was found to carry a novel *de novo* germline mutation in the C-terminus of *SEPT6* (mutation M2), not identified in the trio whole-genome/whole-exome NGS (WGS/WES) analysis of his biological parents. SEPT6 is located on the X chromosome and thus the mutation hemizygous in this boy (*). This mutation was associated with the accumulation of additional pre-malignant clonal aberrations (trisomy 7,8,9) and progressive tetraploidy in the patient's BM. By WES of the patient's pre-HSCT BM, we also we also identified a somatically acquired, low-frequency compensatory frameshift *SEPT6* mutation (M1). Early HSCT was performed to treat the progressive cytopenias and to prevent transformation from MDS to AML. The patient is alive and well without any other hematological or other phenotype 10 years after HSCT. To dissect the putative role of the *SEPT6*-M2 mutation, we generated fibroblast-derived iPSCs from the patient and controls and studied them and their hematopoietic progeny. LOF = loss of function.

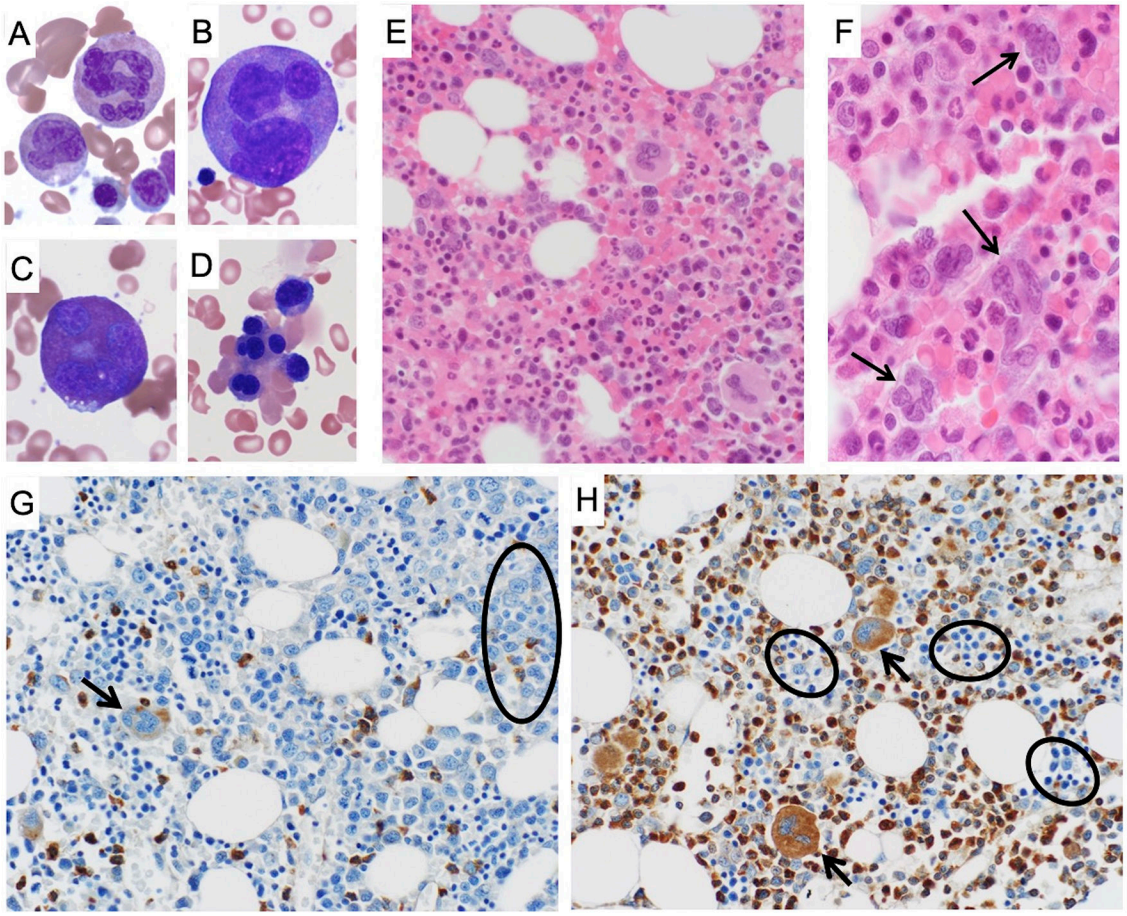

Figure 2: Hematopathological features SEPT6-associated congenital MDS and abnormal bone marrow SEPT6 staining corrected after allogenic HSCT.

Bone marrow aspirate and biopsy of the patient displayed strikingly abnormal myeloid precursors which were diffusely present. In BM aspirates stained by May-Grunwald-Giemsa (MGG, at 40x magnification), we observed giant multinucleated neutrophils (panel A), giant multinucleated promyelocytes (panel B), giant multinucleated eosinophils (panel C). In addition, we noted prominent nuclear lobation in erythroid precursors (panel D). In parallel, similar findings were seen on BM biopsy after hematoxylin & eosin (H&E), confirming the presence of abnormal, giant myeloid progenitors (panel E, 20x magnification) and multinucleated granulocyte precursors (panel F, 40x magnification, arrows). Bone marrow biopsies from the patient were stained after validation of a SEPT6 antibody for immunohistochemistry on an array of normal human tissues (Supplementary Figure S6). In the biopsies stained by MGG prior to HSCT (panel G, at 20x magnification), we observed markedly decreased SEPT6 staining in granulocyte precursors (circle) and megakaryocytes (arrow). This abnormality was corrected in the biopsy post-HSCT (panel H, at 20x magnification), where we noted normal SEPT6 staining of myeloid progenitors and megakaryocytes (arrows), and comparatively decreased erythroid staining (circles).

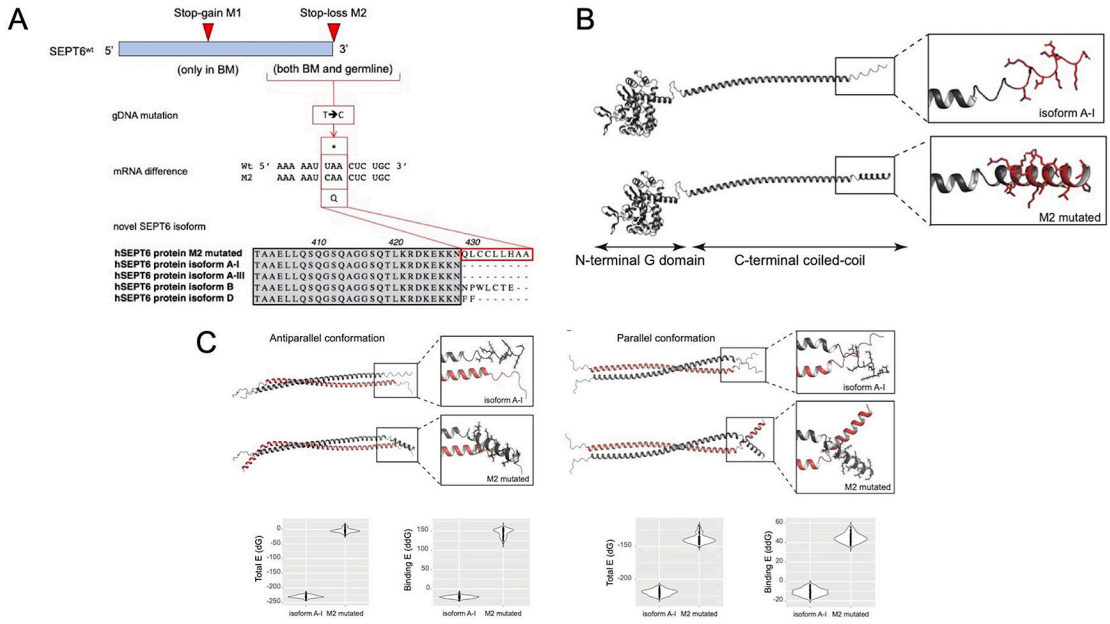

Figure 3: Schematic representation of the mutations identified in SEPT6 and their impact on protein structure

Panel A: Top: *SEPT6* on chromosome Xq24 was found to harbor a germline C-terminal mutation not found in any database of common polymorphisms or disease-associated sequencing datasets (mutation M2, 1282T>C). At low clonal frequency, and only in the patient's BM, we identified an additional stop-gain mutation at low variant allele frequency predicted to represent an acquired somatic compensatory effect by abrogation of the constitutionally expressed M2-mutated SEPT6 pathogenic variant. Middle: The *SEPT6*^{M2} mutation produces a STOP-codon abrogation and the continued transcription of the *SEPT6* gene. Bottom: The novel M2-mutated SEPT6 isoform is 9 aa longer than the main SEPT6 A-isoforms of the protein, and carries hydrophobic residues, similarly to isoforms B and D. Panel B: In silico models of the A-I and M2 isoform coiled-coil domains of SEPT6. Models of the A-I and M2 isoforms of SEPT6 were generated using AlphaFold2. The A-I isoform shows a disordered C-terminal tail, whereas the 9 additional residues of the M2 isoform form a structured motif with helix propensity. Panel C: On the left, modelled monomers were aligned on the crystal structure of antiparallel Septin6 (PDB 6wbp) and evaluated using the Rosetta-ICO energy function. The formation of the antiparallel dimer is more energetically favorable for the wild-type A-I than for the M2 mutated isoform. On the right, modelled monomers were aligned to parallel coiled coils generated using the CCFold web server and evaluated using the Rosetta-ICO energy function [33]. The formation of the parallel dimer is more energetically favorable for the wild-type A-I than for the M2 mutated isoform.

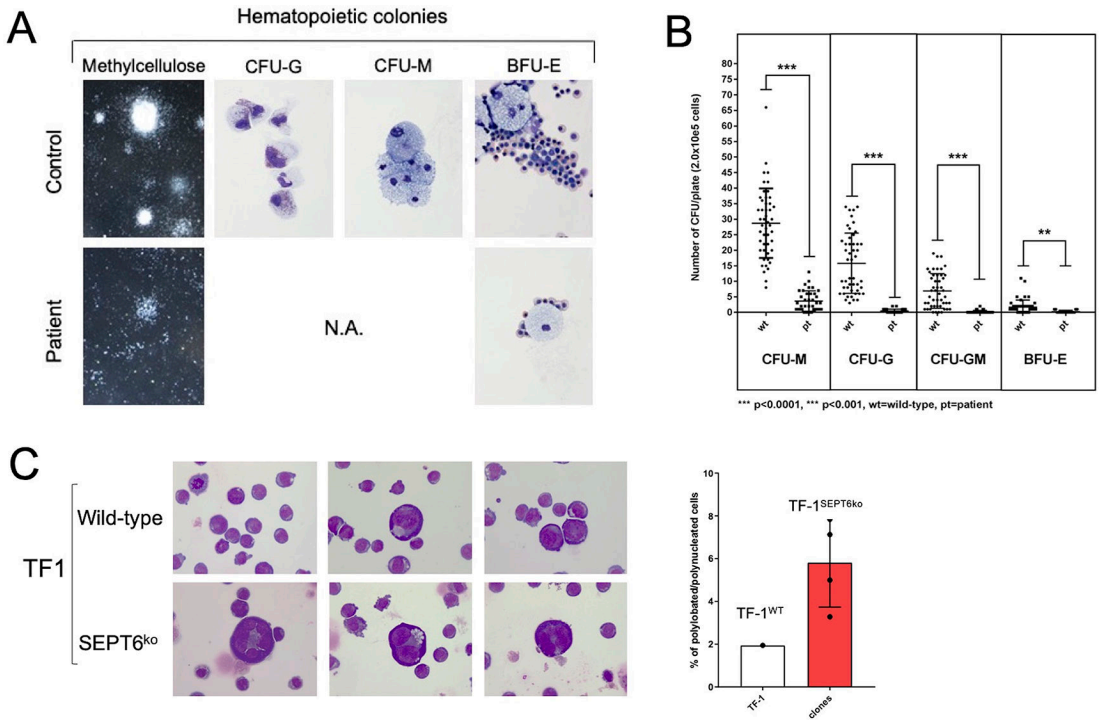

Figure 4: Derivation of hematopoietic progenitors from patient-iPSC colonies phenocopies the hematological findings of SEPT6-associated congenital MDS, and the genetic knock-out of SEPT6 in hematopoietic cell lines reveals a propensity to multinuclearity.

Embryoid bodies (EB) were generated from patient and healthy control iPSCs (Supplementary Figure 2A), which were morphologically comparable. From EBs, hematopoietic progenitor cells (HPCs) were extracted, plated into differentiation-cytokine containing methycellulose (2.0x10e5 cells per 5cm diameter dish), and analyzed at maximal expansion of colony-forming units (CFUs). CFUs were scored by standard microscopical means following morphological guidelines into granulocyte (G), monocyte (M), granulocyte-monocyte (GM) and erythroid (E) categories and counted twice. Larger colonies were aspirated by pipetting and cytospins stained by MGG. Patient-derived CFUs were markedly reduced in numbers and size at maximal expansion in methylcellulose when compared to CFUs from control iPSCs (panel A, left). We generated myeloid lineage progenitors (CFU-G, -GM, -M, -E) from patient-derived iPSC clones at good efficiency, and cellular morphology confirmed to be correct after MGG staining of cytospins of larger representative colonies (panel A, right, 100x magnification). This was not the case for HPCs generated from patient-derived iPSC clones, where colonies were too small to allow morphological confirmation. To numerically quantify the defect, we counted CFUs and observed a defective granulocyte/monocyte development of CFUs from patient-derived iPSCs. We measured a differential effect on the myeloid/granulocyte lineage compared to the erythroid lineage with a reduction by 36-fold in CFU-G, 46-fold CFU-GM, 8-fold in CFU-M, and 6-fold in BFU-E colony output in the patient derived HPC when compared to controls (panel B). Data is from n=3 non-synchronous experiments, pooling iPSC clones (c5 and c8 for patient, c1 and c6 for control). Statistical significance was calculated by Student t-testing. Wt= wild type controls, Pt= patient derived cells, ****p<0.0001, ***p<0.001.

After attempting to knock-in/out *SEPT6* in iPSCs and human granulocytic/myeloid cell lines, which showed an intolerance to *SEPT6* insufficiency, we genetically edited the erythroleukemic cell line TF-1 by CRISPR/Cas9 and achieved a complete *SEPT6* knock-out in pooled cells which remained stable in multiple generations of single cell clones (Supplementary Figure 5A-B). After culture displaying no difference in proliferative dynamics, we noted giant cells with multinucleation in *SEPT6* knock-out clones, when cytospins were stained by MGG, while this could not be seen in wild-type TF-1 controls (panel C left, 40x magnification). To address this observation numerically, we counted nucleated cells by categories (mono-, bi- polynucleation), and identified an increased proportion of larger, multinucleated/lobated cells in *SEPT6* knock-out clones. Data is from n>1000 for each SEPT6 ko clone and wild-type, one experiment representative of three. When *SEPT6* knock-out clone counts were pooled and frequency of multinucleated/lobated cells was compared with wild-type TF-1 cells, a 3-fold increase was observed (panel C right). This population of cells was insufficient to cause differences in DNA content and cell cycle as assayed by flow cytometry after PI/7-AAD staining.